**Supplementary Material for:**

# Iron(II) PARACEST MRI Contrast Agents

Sarina J. Dorazio, Pavel B. Tsitovich, Kevin E. Siters, Joseph A. Spernyak, and Janet R. Morrow

Department of Chemistry, University at Buffalo, State University of New York, Amherst, NY 14260-3000

Department of Cell Stress Biology, Roswell Park Cancer Institute, Buffalo, NY 14263

## Table of Contents

**Materials and methods**.

*Instrumentation***.** All $^{1}$H NMR spectra were acquired using Varian Inova-500 or Inova-400 NMR spectrometers. A Varian Mercury-300 NMR spectrometer was used to acquire all $^{13}$C NMR spectra. Chemical shifts were referenced to residual solvent peaks. Mass spectral data were acquired on a ThermoFinnigan LCQ Advantage IonTrap LC/MS equipped with a Surveyor HPLC system. High-resolution mass spectral data were acquired on a ThermoFinnigan MAT95XL w/ESI II source (NSF Award HE0091977). CEST experiments were acquired on a Varian Inova 400 MHz spectrometer at 25 $^{o}$C or 37 $^{o}$C (as indicated). The pulse power was varied from $B_1$ = 240 to 960 Hz with an irradiation time of either 2 or 4 seconds.

*PARACEST imaging*. CEST images were acquired on a 4.7 Tesla preclinical MR scanner using a 35mm radiofrequency coil and the ParaVision 3.0.2 research platform (Bruker Biospin, Billerica, MA). A pair of gradient-echo MR images were acquired at either 37 $^{o}$C (**L1**) or 22 $^{o}$C (**L2**) with a pre-saturation pulse train comprised of five 1 second Gauss pulses (10μT , 200 μs interpulse delay) applied symmetrically about the bulk water resonance (**L1**: +/- 69ppm, **L2**: +/- 6.5 ppm). Other key acquisition parameters include: echo time/repetition time = 2.1/5010 ms, flip angle = 90 deg, acquisition matrix = 160x160, slice thickness = 2 mm, field of view = 32x32mm, averages = 1.

To determine the CEST effect, each image was normalized to the signal intensity of the buffer-only phantom and the normalized image intensity of each phantom was sampled using commercially available software (Analyze 7.0, AnalyzeDirect Inc., Overland Park, KS). The percent loss of signal due to PARACEST exchange was calculated using the equation: CEST Effect = $1-SI_{on}/SI_{off}$, where $SI_{on}$ is the image intensity of each sample acquired with an on-resonance pre-saturation pulse and $SI_{off}$ is the image intensity acquired with the off-resonance pre-saturation pulse. Results are shown in figure S6. To create the CEST image (figure 2), each data set was first filtered with a spatial low-pass filter (kernel size: 5x5) to improve signal-to-noise, normalized by image intensity of the buffer-only phantom, and then subtracted. Phantoms in the subtraction image were isolated using binary masking techniques, and a "hot-iron" pseudo-color lookup table was applied to enhance visual detection of differences of the CEST effect in phantoms.

*$T_1/T_2$ Relaxivity.* $T_1/T_2$ relaxivity values were determined on a 4.7 Tesla MRI system. $T_1$ relaxation rates of serial dilutions were measured using an inversion-recovery TrueFISP acquisition with the following parameters: TE/TR=1.5/3.0 ms, flip angle=30°, inv. repetition time=10 s, segments=8, frames=100. $T_2$ relaxation rates were measured using a multi-echo, Carr-Purcell-Meiboom-Gill (CPMG) spin-echo sequence with a fixed TR of 3000 ms and TE times ranging from 20-1200 ms in 20 ms increments (60 echoes). The relaxation rate of each sample calculated using non-linear regression analysis routines developed in Matlab (MathWorks, Natick, MA) and relaxivities were then calculated by linear regression (concentration vs. relaxation rate). Results are reported in Table S4.

*Determination of magnetic moment.* The Evans' method[1] was used to determine the effective magnetic moment in the solution state by $^1$H NMR. The paramagnetic complex was dissolved in $D_2O$ containing 5% t-butanol (by volume) as an inert reference standard. This sample was placed in a coaxial insert tube. The outer 5 mm NMR tube contained only $D_2O$ and 5% t-butanol as a diamagnetic reference. Two signals appear for t-butanol in the $^1$H NMR spectrum; one signal is shifted due to the presence of paramagnetic substance while the other serves as a diamagnetic reference. From this chemical shift difference, the following equation can be used to determine mass susceptibility:[2]

$$\chi_g = (-3\Delta f)/(4\pi fm) + \chi_o + [\chi_o (d_o - d_s)]/m \qquad \text{Eq. S1}$$

Here, $\chi_g$ is mass susceptibility of the solute {[Fe(**L1**)]$^{2+}$ or [Fe(**L2**)]$^{2+}$ } in cm$^3$/g, $\Delta f$ is the observed frequency shift between diamagnetic and paramagnetically shifted reference standard in Hz, $f$ is the spectrometer frequency in Hz, $m$ is the mass of substance (per cm$^3$ of solution), and $\chi_o$ is the mass susceptibility of the solvent (cm$^3$/g). The literature value for mass susceptibility of $D_2O$ ($\chi_o$ = -0.6466 x 10$^{-6}$ cm$^3$/g) was used.[3] The third term contributes little to the overall determination and may be neglected. If included, $d_o$ is density of the solvent and $d_s$ is density of the solution in g/cm$^3$.

The calculated $\chi_g$ value is multiplied by the molecular weight of the paramagnetic complex to convert to $\chi_m$, the molar susceptibility (cm$^3$/mol). From this, the effective magnetic moment ($\mu_{eff}$) is determined in relation to temperature in units of Kelvin:

$$\mu_{eff} = 2.84 (\chi_m T)^{1/2} \qquad \text{Eq. S2}$$

At 25 $^{o}$C, values of $\mu_{eff}$ = 5.1 and 5.8 Bohr magnetons for [Fe(**L1**)]$^{2+}$ and [Fe(**L2**)]$^{2+}$, respectively, were obtained. The value for [Fe(**L1**)]$^{2+}$ is within range of that reported for high spin Fe(II) while the value for [Fe(**L2**)]$^{2}$ is slightly higher.[4,5] This is possibly due to a small amount of high spin Fe(III) contaminant. However, $^{1}$H NMR calibration of the samples versus a standard shows that the compounds are predominantly Fe(II). Note also that only Fe(II) complexes have the sharp proton resonances that give rise to the PARACEST spectra.

*HPLC Purification.* Reversed-phase high-performance liquid chromatography (HPLC) purification was accomplished using Waters 1525 Binary HPLC Pump equipped with a Waters 2487 Dual λ Absorbance Detector system. Compounds **iv** and **L2** (Scheme S1) were HPLC-purified using a preparative C8 column (7 μm, 19×150 mm). A linear gradient of solvent B (0.1% TFA in methanol) in solvent A (0.1% TFA in water) at constant flow rate of 8 mL/min was used for HPLC purification.

*Materials.* 3-Nitro-2,6-lutidine and *N*-bromosuccinimide, 99%, (NBS) were obtained from Thermo Fisher Scientific (Waltham, MA). 2,2'-Azobisisobutyronitrile, 98%, (AIBN) and 1,4,7-triazacyclononane, 98%, (TACN) were purchased from Sigma-Aldrich (St. Louis, MO). All chemicals and solvents were used as received if not otherwise noted.

**Synthetic Methods.**

1,4,7-Tris(carbamoylmethyl)-1,4,7-triazacyclononane (**L1**) was prepared as reported previously.[6] 1,4,7-Tris(2-pyridylmethyl)-1,4,7-triazacyclononane (**L3**) was synthesized according to the reported procedure.[7]

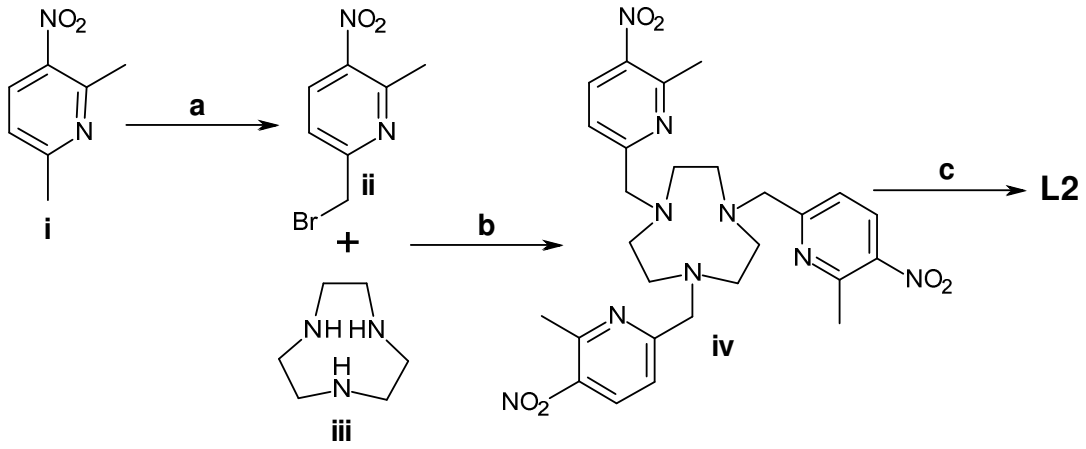


**Scheme S1.** Synthesis of **L2**. *Reagents and conditions:* (a) NBS, AIBN, carbon tetrachloride, 50 °C to reflux, Ar, 8 h; (b) TEA, acetonitrile, 50 °C, 24 h; (c) hydrogen, 10% Pd/C, methanol, 8 h.

**1.1. Synthesis of 6-(bromomethyl)-2-methyl-3-nitropyridine (ii).** 3-Nitro-2,6-lutidine **i** (2.50 g, 16.5 mmol, 1 equiv.) was dissolved in 200 mL of argon-purged carbon tetrachloride. The reaction mixture was heated to 50 °C under argon. AIBN (0.14 g, 0.83 mmol, 5 mol%) was added to the reaction mixture in one portion under constant stirring, followed by the addition of NBS (2.93 g, 16.5 mmol, 1 equiv.) in small portions over a period of 2 h. The reaction mixture was further refluxed for 8 h at constant stirring and under light irradiation. Once the reaction was complete, solvent was removed *in vacuo* producing a brownish residue. This residue was suspended in a mixture of methanol-dichloromethane, in which non-dissolved solids were removed by filtering through a $SiO_2$ plug (ca. 120 mL) using an eluent of methanol-dichloromethane (1:20 v/v). Fractions containing **ii** were combined and solvent was removed *in vacuo*. Resultant oil was subject to $SiO_2$ column chromatography using a mixture of ethyl acetate (gradient from 2% to 10%) in hexanes as an eluent. Fractions containing product were concentrated *in vacuo* producing analytically pure **ii**. Yield: 0.41 g, 1.78 mmol, 11%. $^1$H NMR, 500 MHz ($CDCl_3$, ppm): δ = 8.26 d (1H, Ar, J = 9 Hz), 7.47 d (1H, Ar, J = 9 Hz), 4.52 s (2H, $CH_2$), 2.83 s (3H, $CH_3$). $^{13}$C NMR, 75 MHz ($CDCl_3$, ppm): δ = 160.46, 153.73, 144.66, 133.66, 121.61, 32.07, 23.84. ESI-MS (m/z): $[M+H]^+$, calculated: 231.0, found: 231.0.

**1.2. Synthesis of 1,4,7-tris[(6-methyl-5-nitro-2-pyridyl)methyl]-1,4,7-triazacyclononane (iv).** 1,4,7-Triazacyclononane **iii** (41 mg, 0.32 mmol, 1 equiv.) and alkylating agent **ii** (258 mg, 1.12 mmol, 3.5 equiv.) were dissolved in 8 mL of dry acetonitrile followed by addition of triethylamine (180 µL, 1.29 mmol, 4 equiv.). The reaction mixture was stirred at 50 °C for 24

hours under argon. Upon completion of the reaction, solvent was removed *in vacuo* producing a brown oily residue. The crude product was purified by reversed-phase HPLC using a gradient of solvent B from 30% to 70% in solvent A over 40 min. ESI-MS analyses of fractions with retention time $t_R$ = 21 min confirmed product **iv**. These fractions were combined and solvent was removed by lyophilization producing **iv** in the form of TFA salt. Yield: 80 mg, 63 µmol, 20%. $^1$H NMR, 500 MHz ($CD_3OD$, ppm): δ = 8.35 d (3H, Ar, J = 9 Hz), 7.55 d (3H, Ar, J = 9 Hz), 4.32 s (6H, $3CH_2$), 3.23 m (12H, $6CH_2$), 2.78 s (9H, $3CH_3$). $^{13}$C NMR, 75 MHz ($CD_3OD$, ppm): δ = 160.60, 154.51, 146.59, 134.91, 123.40, 60.07, 50.74, 23.92. High-resolution ESI-MS (m/z): $[M+H]^+$, calculated: 580.2627, found: 580.2691.

**1.3. Synthesis of 1,4,7-tris[(5-amino-6-methyl-2-pyridyl)methyl]-1,4,7-triazacyclononane (L2).** TFA salt of compound **iv** (80 mg, 63 µmol) was dissolved in 40 mL of methanol containing 21 mg (11 mol%) of 10% Pd/C. Reduction of nitro groups was carried out in a Parr hydrogenation apparatus for 8 h using hydrogen gas. Once reduction was complete, the reaction mixture was filtered through Celite. The solvent was removed *in vacuo* producing yellow oil. The crude product was HPLC-purified using a gradient of solvent B (5% to 35%) in solvent A over 30 min. ESI-MS analyses of fractions with retention time $t_R$ = 11 min confirmed product **L2**. These fractions were combined and solvent was removed by lyophilization producing **L2** in the form of TFA salt. The product was further desalted by passing through 2 mL of Dowex® 1×2-100 strongly basic anion exchange resin. The resulting aqueous solution was concentrated *in vacuo* producing **L2**. Yield: 12.6 mg, 26 µmol, 41%. $^1$H NMR, 500 MHz ($D_2O$, pH 7.0, ppm): δ = 7.10 d (3H, Ar, J = 9 Hz), 6.77 d (3H, Ar, J = 8 Hz), 3.77 s (6H, $3CH_2$), 2.75-2.95 m (12H, $6CH_2$), 2.35 s (9H, $3CH_3$). High-resolution ESI-MS (m/z): $[M+H]^+$, calculated: 490.3374, found: 490.3385.

**Table S1.** Overview of characterization methods used for complexes.

| Characterization Method | Fe(L1) | Fe(L2) | Fe(L3) |
|---|---|---|---|
| 1D $^{1}$H NMR: $CD_3CN$ & $D_2O$ | x | x | |
| NMR: PARACEST, 25 $^{o}$C | x | x | |
| NMR: PARACEST, 37 $^{o}$C | x | x | |
| Phantom Image, 25 $^{o}$C | x | x | |
| Phantom Image, 37 $^{o}$C | x | | |
| pH Potentiometrics (log K) | x | | x |
| $T_1$ & $T_2$ Relaxivity | x | x | |
| Magnetic Moment (Evans') | x | x | |

**Table S2**. Acid-dissociation constants (p$K_a$) and ligand–Fe(II) equilibrium constants for **L1** and **L3** for solutions containing 1.05 mM of **L1** or **L3** and 1.0 mM $Fe(OTf)_2$, 0.10 M NaCl, at 25°C.

| **Equilibrium** | **Fe(L1)** | **Fe(L3)** |
|---|---|---|
| Log $K_1$ | 10.19 ± 0.11 | 12.20 ± 0.81 |
| Log $K_2$ | < 2 | 4.6 ± 0.50 |
| Log $K_3$ | < 2 | < 2 |
| Log $K_4$ | N/A | < 2 |
| Log $K_5$ | N/A | 3.93 ± 0.64 |
| Log $K_6$ | N/A | 2.33 ± 0.21 |
| Log $K_{Fe\text{-}L}$ | 13.47 ± 0.25 | 19.24 ± 0.64 |
| Log $K_{Fe\text{-}LH}$ | 5.54 ± 0.14 | 4.8 ± 0.87 |
| Log $K_{FeL\text{-}OH}$ | 9.43 ± 0.18 | 10.15 ± 1.35 |

The Protonic Software program Hyperquad 2008 was used to fit potentiometric data and derive equilibrium constants. Corresponding equilibrium equations and expressions are included in Table S3.

**Table S3**. Equilibrium Expressions for L = **L1** or **L2**.

| | |
|---|---|
| Eq. 1 | $L + H^+ \leftrightarrows LH^+$ |
| | $K_1 = [LH^+]/([L][H^+])$ |
| Eq. 2 | $LH^+ + H^+ \leftrightarrows LH_2^{2+}$ |
| | $K_2 = [LH_2^{2+}]/([LH^+][H^+])$ |
| Eq. 3 | $LH_2^{2+} + H^+ \leftrightarrows LH_3^{3+}$ |
| | $K_3 = [LH_3^{3+}]/([LH_2^{2+}][H^+])$ |
| Eq. 4 | $LH_3^{3+} + H^+ \leftrightarrows LH_4^{4+}$ |
| | $K_4 = [LH_4^{4+}]/([LH_3^{3+}][H^+])$ |
| Eq. 5 | $LH_4^{4+} + H^+ \leftrightarrows LH_5^{5+}$ |
| | $K_5 = [LH_5^{5+}]/([LH_4^{4+}][H^+])$ |
| Eq. 6 | $LH_5^{5+} + H^+ \leftrightarrows LH_6^{6+}$ |
| | $K_6 = [LH_6^{6+}]/([LH_5^{5+}][H^+])$ |
| Eq. 7 | $L + Fe^{2+} \leftrightarrows FeL^{2+}$ |
| | $K_{FeL} = [FeL^{2+}]/([Fe^{2+}][L])$ |
| Eq. 8 | $FeL^{2+} + H^+ \leftrightarrows FeLH^{3+}$ |
| | $K_{FeLH} = [FeLH^{3+}]/([FeL^{2+}][H^+])$ |
| Eq. 9 | $FeL^{2+} + OH^- \leftrightarrows FeL\text{-}OH^+$ |
| | $K_{FeL\text{-}OH} = [FeL\text{-}OH^+]/([FeL^{2+}][OH^-])$ |

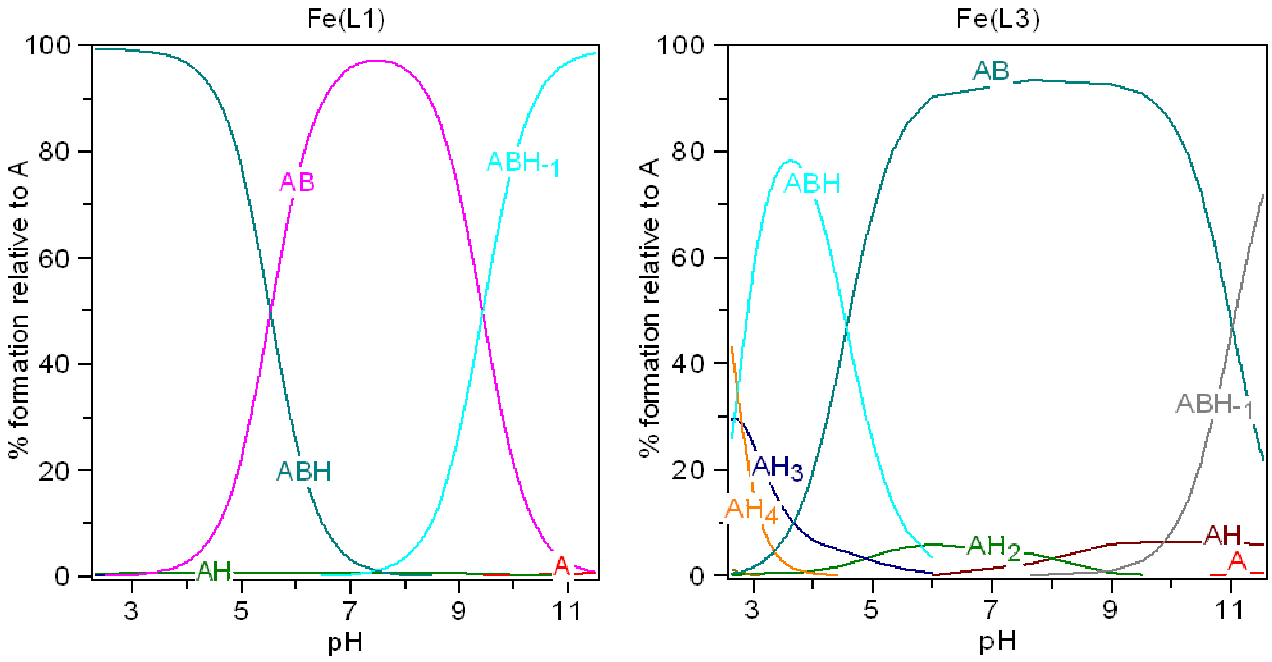


Fe(**L1**) Fe(**L3**)

**Figure S1**. Speciation diagrams. Let A = **L1** or **L3**, B = Fe(II), H = $H^+$, $H_{-1}$ = $OH^-$. Diagrams were derived using the Protonic Software program HySS 2008. Conditions used to determine speciation are identical to those used to determine equilibrium constants.

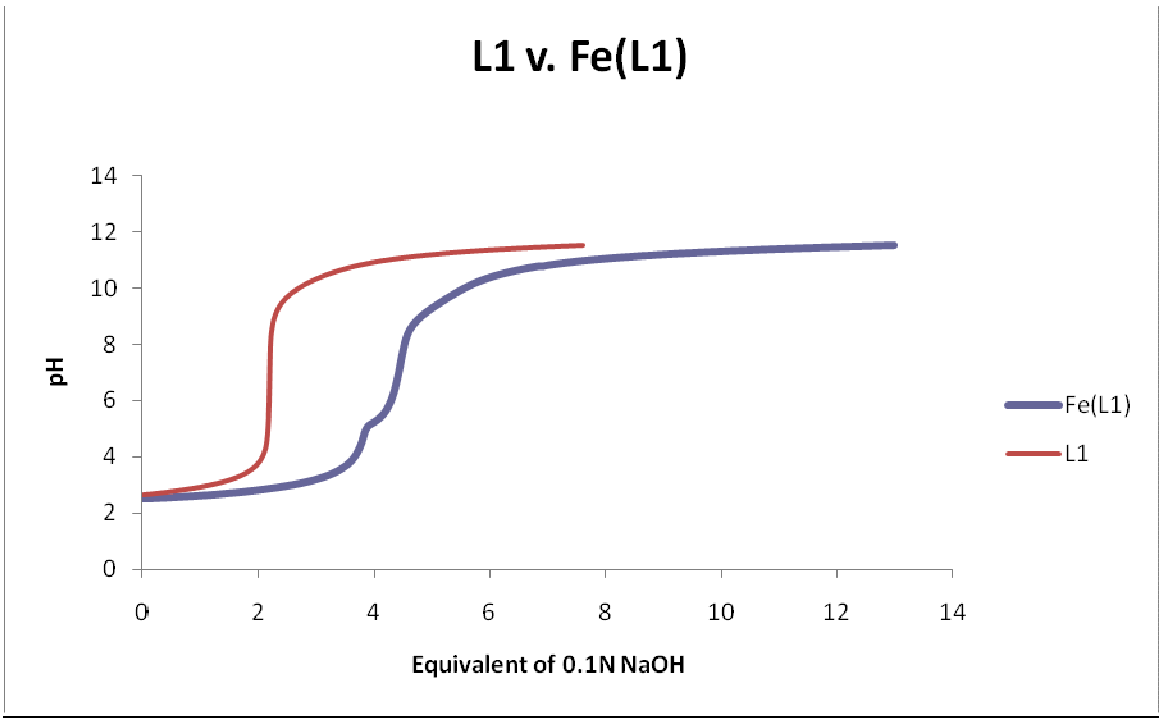


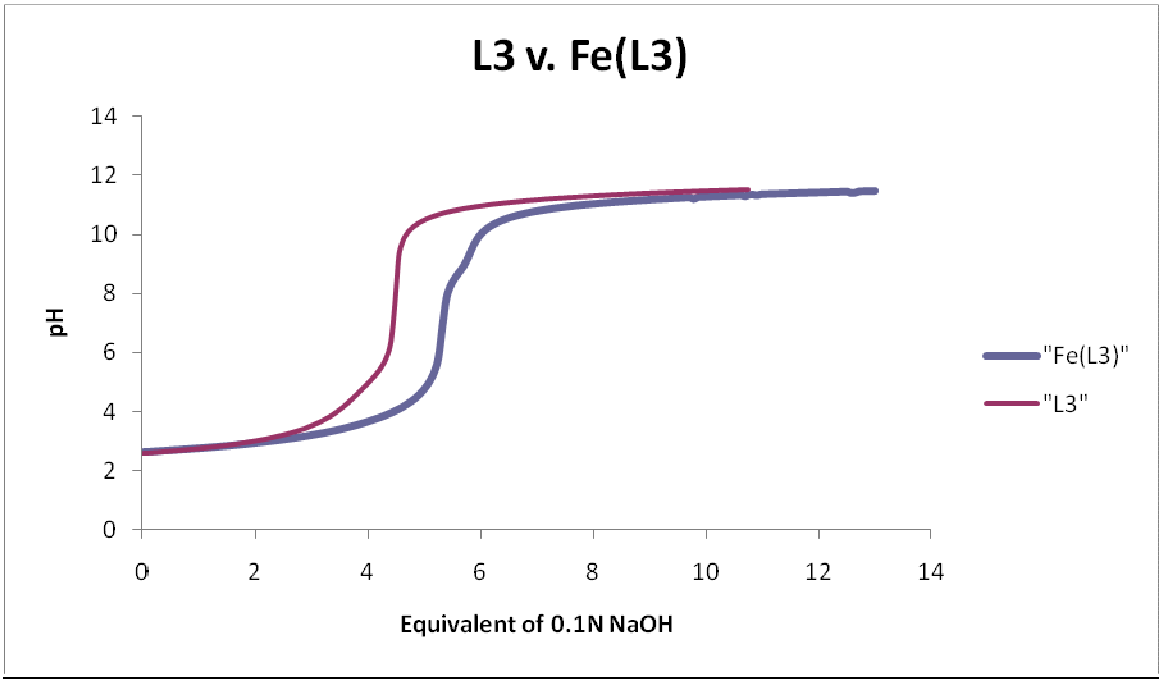


**Figure S2.** pH-potentiometric titrations for Fe(**L1**) and Fe(**L3**) in 100 mM NaCl, 25 $^{o}$C.

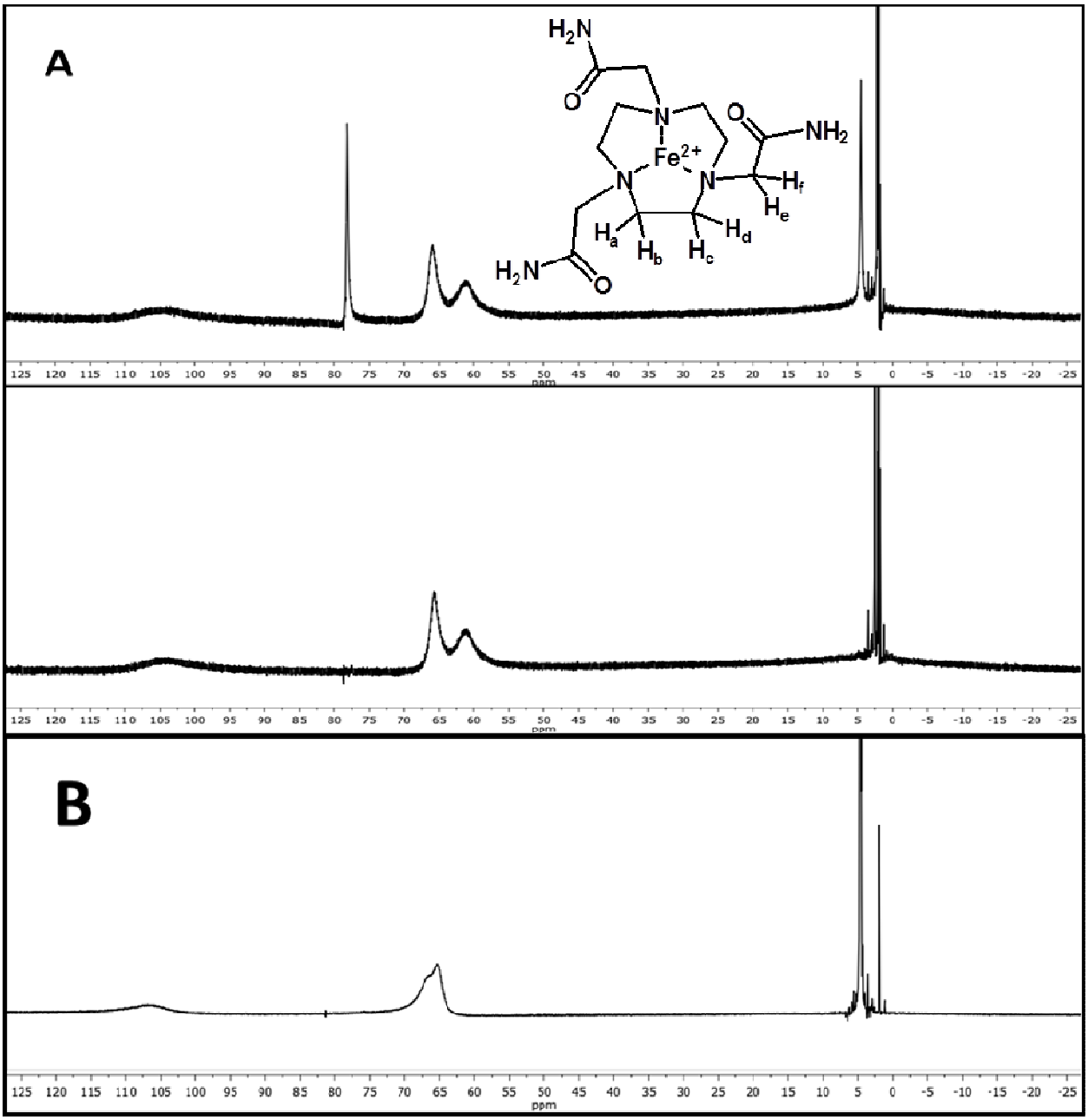


**Figure S3**. 400 MHz $^1$H NMR at 25 $^o$C of $[Fe(\mathbf{L1})]^{2+}$: (**A**) 5.2 mM $[Fe(\mathbf{L1})]^{2+}$ in $CD_3CN$ (top); upon addition of 30 μL $D_2O$ (bottom). The proton resonances at 78.2 ppm and 4.5 ppm in **A** disappear when $D_2O$ is added, indicating location of the exchangeable amide protons of **L1**. The spectrum (**B**) contains 21.3 mM $[Fe(\mathbf{L1})]^{2+}$ in $D_2O$ at pH 6.7, verifying absence of amide peaks and remaining peaks of dynamic $CH_2$. The fact that the six inequivalent non-exchangeable protons as shown in the drawing give rise to three broad peaks is consistent with a dynamic process that exchanges the protons in the pendent group, the protons on the macrocycle closest to the Fe(II), and the protons facing away from the Fe(II) to give three sets of broad peaks.

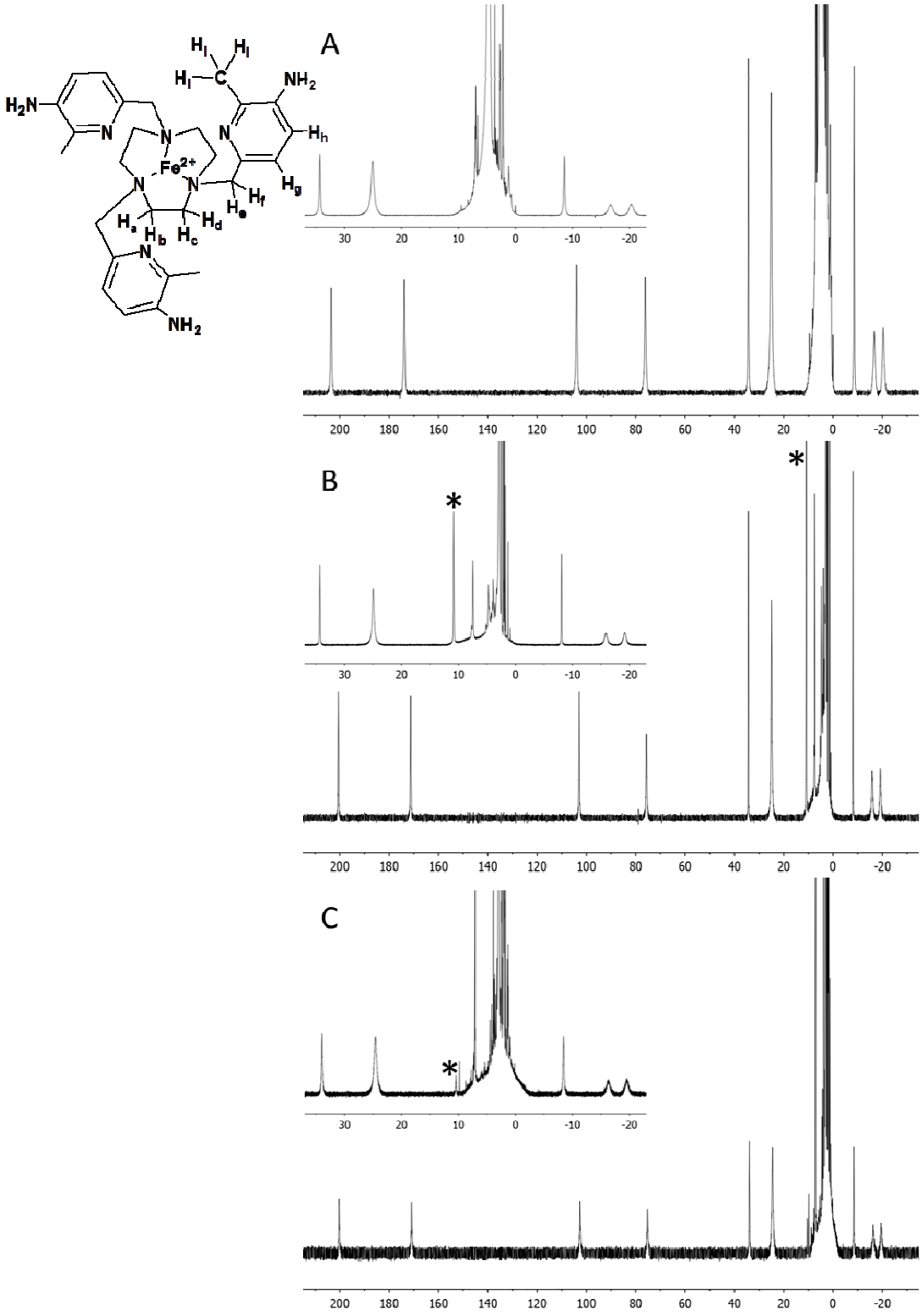


**Figure S4.** $^{1}$H NMR spectra of [Fe(**L2**)]$^{2+}$ in: (**A**) $D_2O$; (**B**) $CD_3CN$; (**C**) $CD_3CN$ containing 5% $D_2O$. Asterisks indicate peaks corresponding to exchangeable amino protons. Drawing shows the nine inequivalent non-exchangeable protons whose assignments have not yet been made.

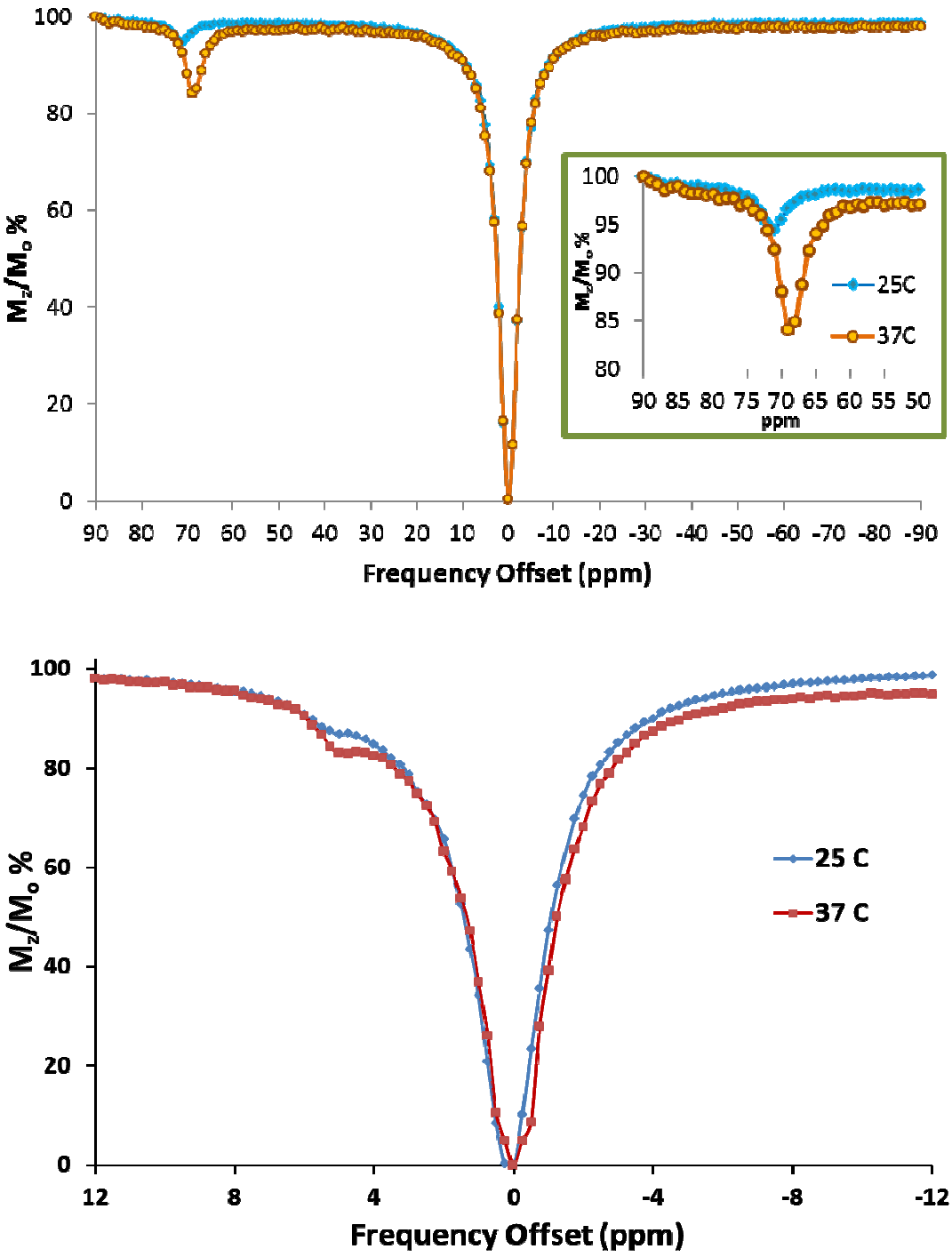


**Figure S5.** CEST recorded at 400 MHz of solutions containing 20 mM HEPES, 100 mM NaCl, saturation applied for 4 seconds or 2 seconds, for $[Fe(\mathbf{L1})]^{2+}$ and $[Fe(\mathbf{L2})]^{2+}$, respectively. *Top*: 8 mM $[Fe(\mathbf{L1})]^{2+}$, $B_1$ = 960 Hz; *Bottom*: 4 mM $[Fe(\mathbf{L2})]^{2+}$, $B_1$ = 305 Hz. Inset shows the difference in CEST effect more clearly, in which maximum CEST is observed at 71 ppm at 25 $^{o}$C and 69 ppm at 37 $^{o}$C.

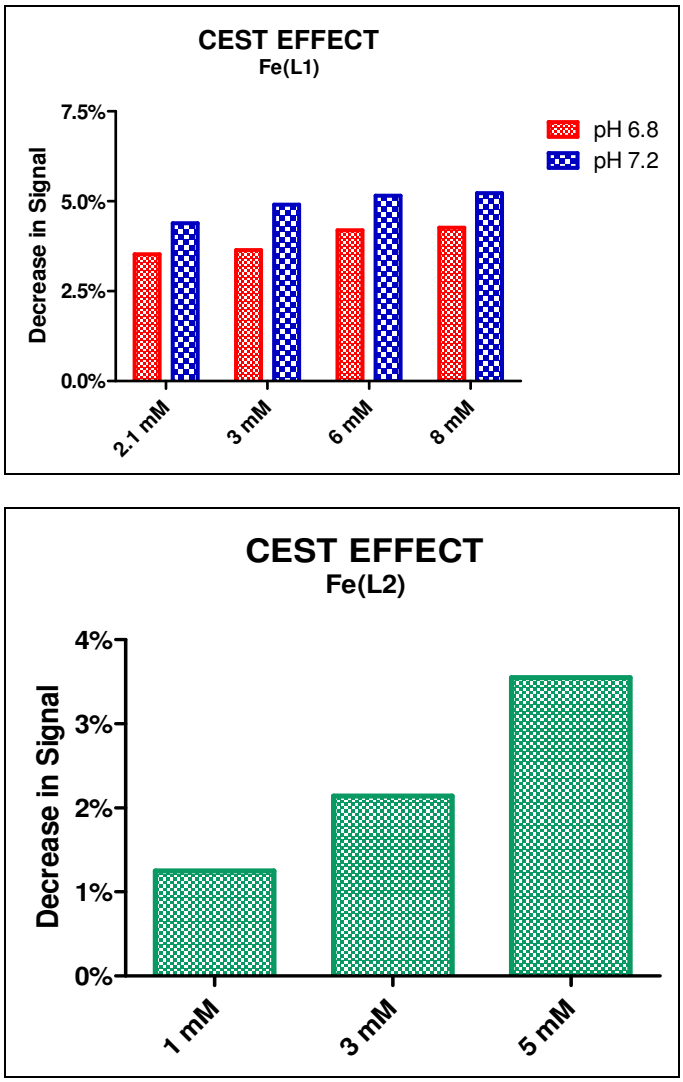


**Figure S6.** Top: Plot of the CEST effect of [Fe(**L1**)]$^{2+}$ at 37 $^{o}$C, 20 mM HEPES, 100 mM NaCl. Bottom: CEST Effect of [Fe(**L2**)] $^{2+}$ at 22 $^{o}$C, 20 mM HEPES, 100 mM NaCl, pH 7.0.

**Table S4**: $T_1$ and $T_2$ relaxivities of Fe(**L1**) $^{2+}$ and Fe(**L2**) $^{2+}$ at 4.7 Tesla. $^{\dagger}$data acquired at 22 $^{o}$C.

| | $T_1$ Relaxivity (mM · s)$^{-1}$ | | $T_2$ Relaxivity (mM · s)$^{-1}$ | |
|---|---|---|---|---|
| Agent | 25°C | 37°C | 25°C | 37°C |
| **Fe(L1)**$^{2+}$ (pH 6.8) | 0.208 | 0.201 | 0.305 | 0.272 |
| **Fe(L1)**$^{2+}$ (pH 7.2) | 0.212 | 0.202 | 0.279 | 0.260 |
| **Fe(L2)**$^{2+}$ (pH 7.0) | 0.021$^{\dagger}$ | - | 0.14$^{\dagger}$ | - |

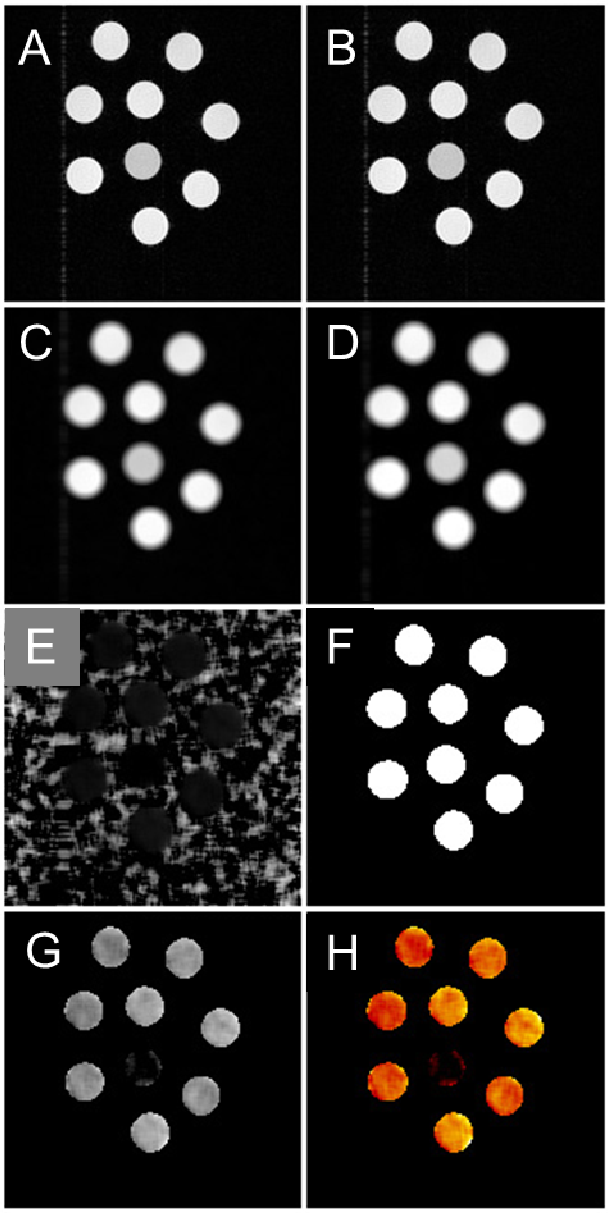


**Figure S7.** Graphical representation of post-processing of PARACEST images of **L1**. MR images were acquired with a 10 μT saturation prepulse off-resonance (A) and on-resonance (B). To increase signal-to-noise, each image was filtered with a 5x5 low-pass averaging filter, yielding panels C & D. A PARACEST image was calculated using equation $1\text{-}SI_{(C)}/SI_{(D)}$ on a voxel-by-voxel basis in Matlab, where SI represents the signal intensity, yielding panel E. To improve visualization, the CEST image was multiplied by a binary representation of the sample tubes (F), yielding panel G. Finally, to accentuate differences in CEST contrast between concentrations and pH formulations, a "hot-iron" lookup table was applied, yielding panel H.

***References: Supplementary Material***


1. Evans, D.F. *J. Chem. Soc.* **1959**, 2003 – 2005.
2. Schubert, E.M. *J. Chem. Ed.* **1992**, 69(1): 62.
3. Iskenderian, H.P. *Phys. Rev.* **1937**, 51(12): 1092 – 1096.
4. Crabb, E.; Moore, E.; Smart, L. *Concepts in Transition Metal Chemistry*; Royal Society of Chemistry: Cambridge 2010.
5. Burger, K. Coordination Chemistry: Experimental Methods; Butterworth: London 1973.
6. Amin, S.; Marks, C.; Toomey, L.M.; Churchill, M.R.; Morrow, J.R. *Inorg. Chim. Acta* **1996**, 246: 99 – 107.
7. Christiansen, L.; Hendrickson, D. N.; Toftlund, H.; Wilson, S. R.; Xie, C. L. *Inorg. Chem*., **1986**, 25, 2813–2818.

# Appendix: Characterization of L2 and Intermediates

## Spectroscopic data for compound ii:

$^1$H NMR of compound **ii** in $CDCl_3$:

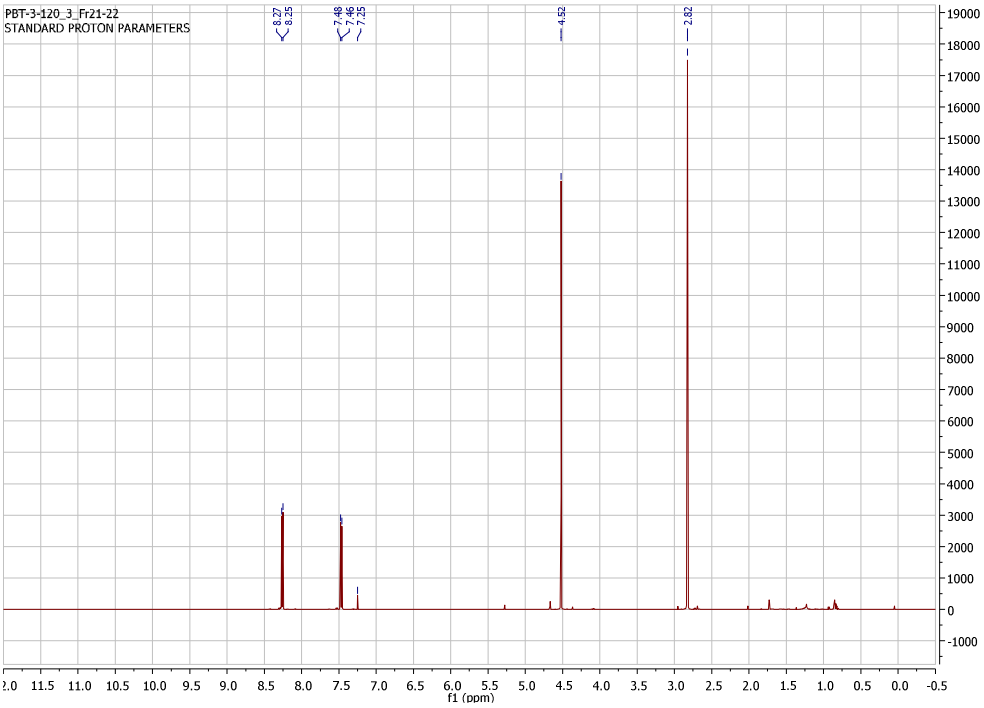


ESI-MS of compound **ii**:

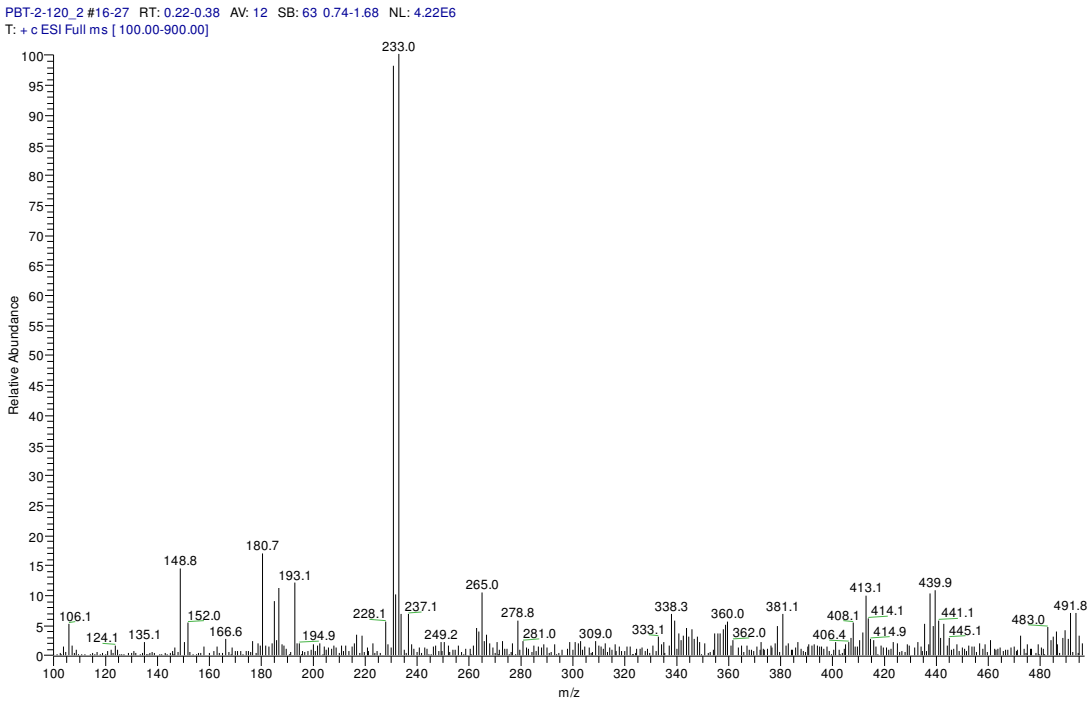

## Spectroscopic data for compound iv:

$^{1}$H NMR of compound **iv** in $CD_3OD$:

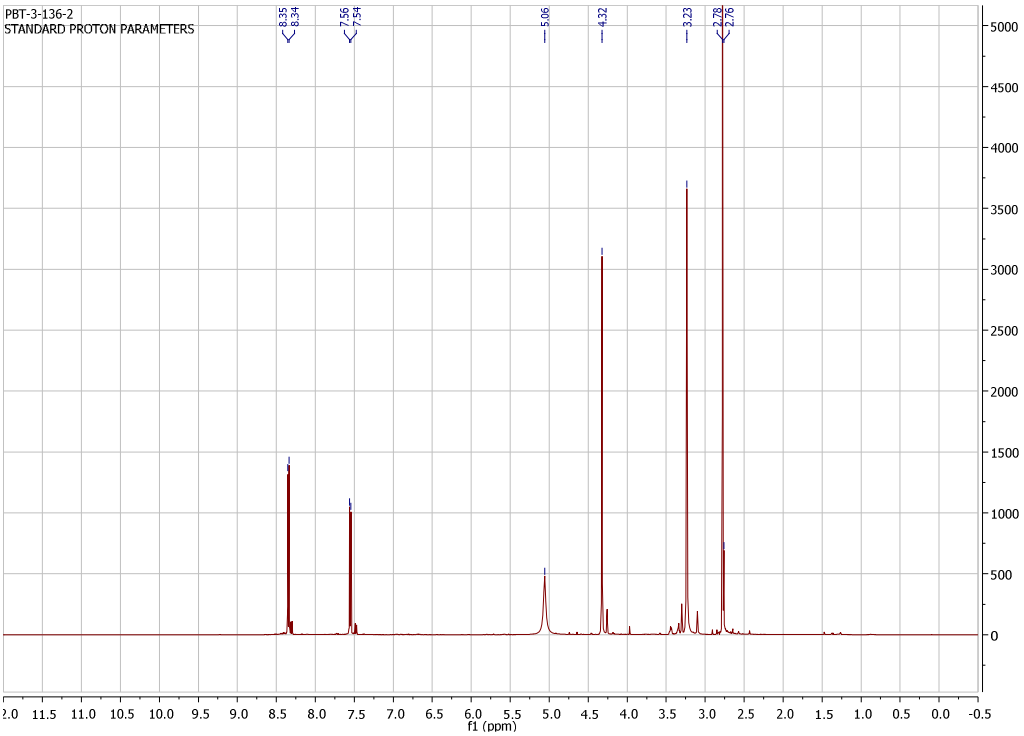


$^{13}$C NMR of compound **iv** in $CD_3OD$:

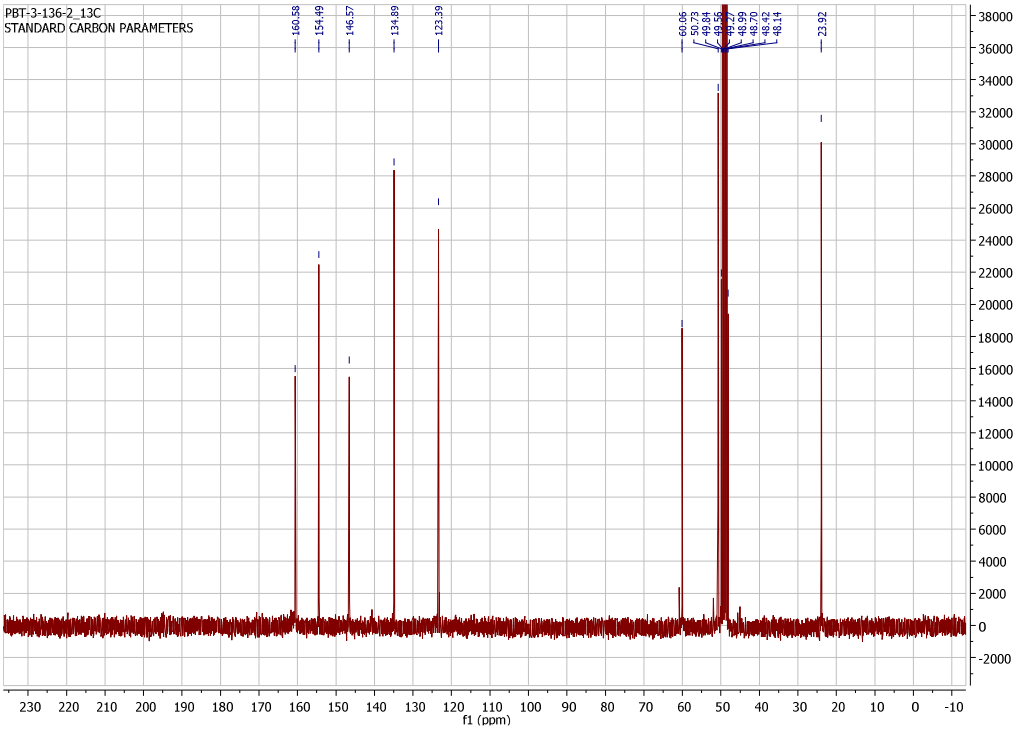

High-resolution ESI-MS of compound **iv**:

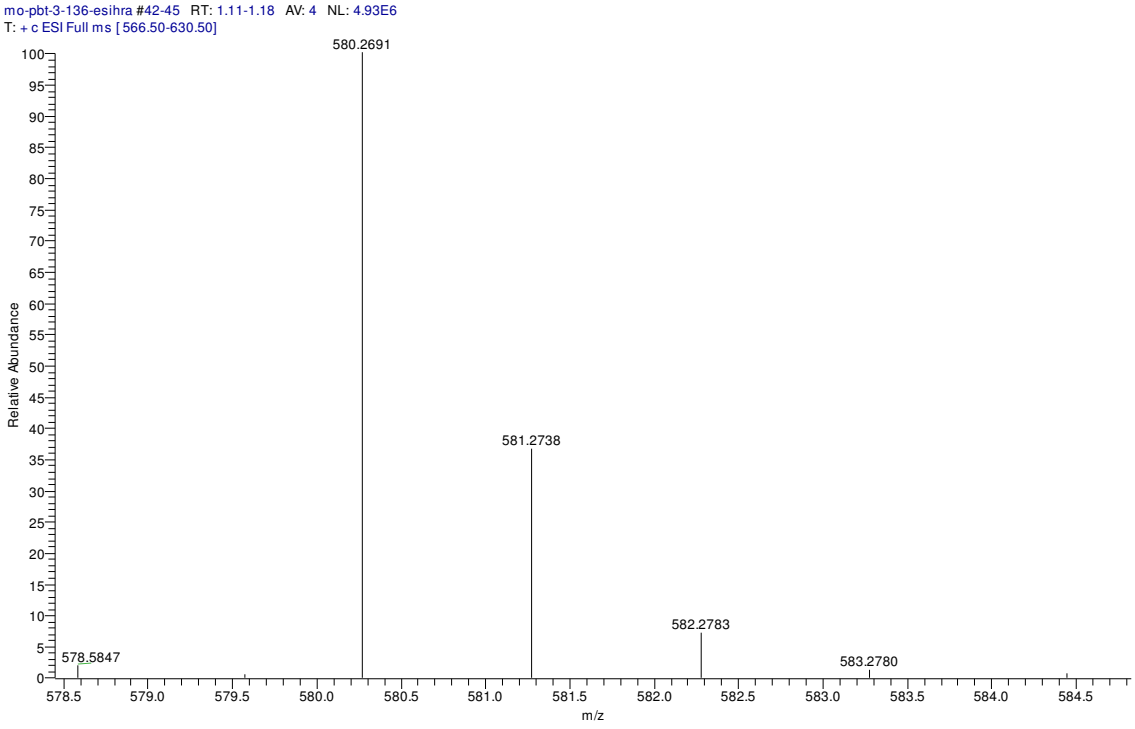

## Spectroscopic data for compound L2:

$^1$H NMR of **L2** in $D_2O$:

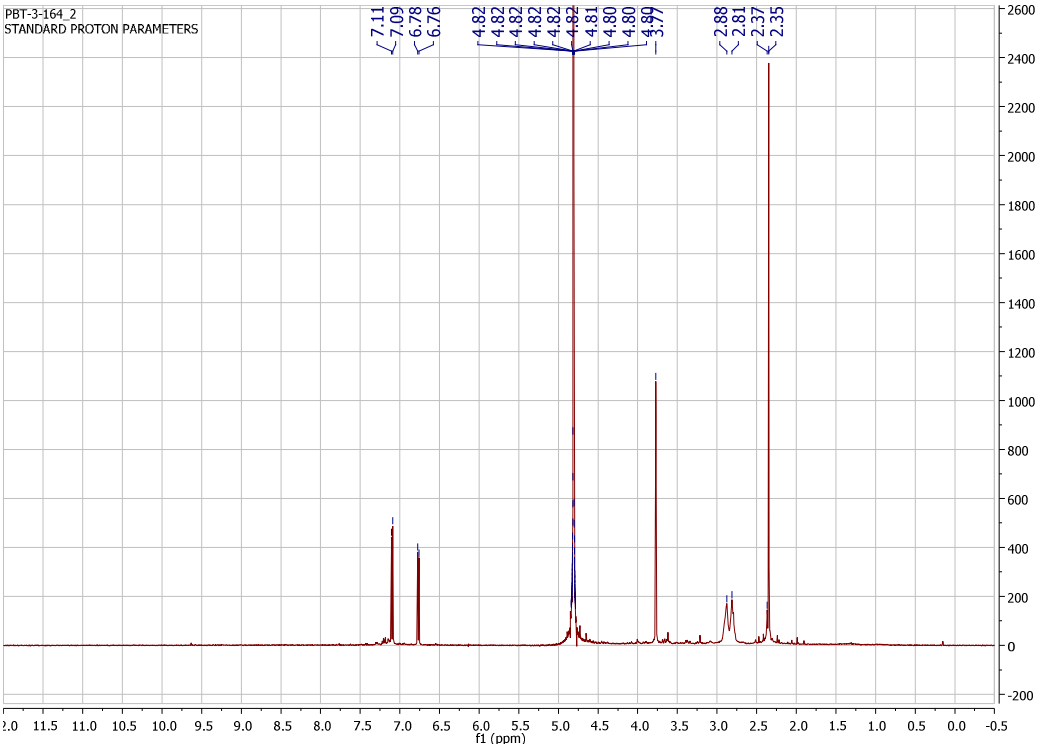


High-resolution ESI-MS of compound **L2**: